

## The ANTICS Large-N Seismic Deployment in Albania

Hans Agurto-Detzel<sup>1\*</sup>, Andreas Rietbrock<sup>1</sup>, Frederik Tilmann<sup>2,3</sup>, Edmond Dushi<sup>4</sup>, Michael Frietsch<sup>1</sup>, Ben Heit<sup>2</sup>, Sofia-Katerina Kufner<sup>1,5</sup>, Mike Lindner<sup>6,7</sup>, Besian Rama<sup>4</sup>, Bernd Schurr<sup>2</sup>, Xiaohui Yuan<sup>2</sup>

<sup>(1)</sup> Karlsruhe Institute of Technology, Geophysical Institute, Germany

<sup>(2)</sup> Deutsches GeoForschungsZentrum (GFZ), Potsdam, Germany

<sup>(3)</sup> Freie Universität Berlin, Germany

<sup>(4)</sup> Department of Seismology, Institute of Geosciences, Polytechnic University of Tirana, Albania

<sup>(5)</sup> Now at GeoZentrum Nordbayern, Friedrich-Alexander University Erlangen-Nürnberg, Germany

<sup>(6)</sup> DESY, Notkestraße 85, 22607 Hamburg, Germany

<sup>(7)</sup> Deutsches Zentrum für Astrophysik, Postplatz 1, 02826 Görlitz, Germany

\* Corresponding author: [hans.detzel@kit.edu](mailto:hans.detzel@kit.edu)

### Important Notice

This manuscript is a non-peer reviewed preprint submitted to EarthArXiv. Subsequent versions of this manuscript may have slightly different content.

December 08, 2024

1  
1  
2  
  
3  
  
4  
  
5  
6  
7  
  
8  
9  
10  
11  
12  
13  
14  
15  
16

# The ANTICS Large-N Seismic Deployment in Albania

Hans Agurto-Detzel<sup>1\*</sup>, Andreas Rietbrock<sup>1</sup>, Frederik Tilmann<sup>2,3</sup>, Edmond Dushi<sup>4</sup>,  
Michael Frietsch<sup>1</sup>, Ben Heit<sup>2</sup>, Sofia-Katerina Kufner<sup>1,5</sup>, Mike Lindner<sup>6,7</sup>, Besian Rama<sup>4</sup>,  
Bernd Schurr<sup>2</sup>, Xiaohui Yuan<sup>2</sup>

- <sup>(1)</sup> Karlsruhe Institute of Technology, Geophysical Institute, Germany
- <sup>(2)</sup> Deutsches GeoForschungsZentrum (GFZ), Potsdam, Germany
- <sup>(3)</sup> Freie Universität Berlin, Germany
- <sup>(4)</sup> Department of Seismology, Institute of Geosciences, Polytechnic University of Tirana, Albania
- <sup>(5)</sup> Now at GeoZentrum Nordbayern, Friedrich-Alexander University Erlangen-Nürnberg, Germany
- <sup>(6)</sup> DESY, Notkestraße 85, 22607 Hamburg, Germany
- <sup>(7)</sup> Deutsches Zentrum für Astrophysik, Postplatz 1, 02826 Görlitz, Germany

Article history: received Month DD, YYYY; accepted Month DD, YYYY

## Abstract

Located within the active continental collision between Eurasia and the Adriatic microplate, Albania is an earthquake prone country with one of the highest seismic hazard in Europe. This came into evidence when the  $M_w=6.4$  Durrës earthquake hit the country in 2019, causing 51 fatalities and widespread damage to infrastructure. Despite this stark reminder, the seismotectonics of Albania remains poorly researched, holding many unknowns regarding active seismogenic faults and 3D velocity structure. In an attempt to fill-in this knowledge gap, we conceived the project ANTICS (AlbaniaN TectonIcs of Continental Subduction) to install a temporary network of 382 seismic stations, and densely monitor the abundant seismic activity in central Albania. In this paper we introduce the project goals and seismic deployment, assessing data quality and extracting valuable lessons from such a complex large-N deployment. Finally, we present some preliminary results on the detected seismicity and a receiver function profile, and expand on an outlook of the project and possible next steps in the area.

Keywords: large-N seismology; Albania; Adriatic Plate; seismic network; seismotectonics

## 1. Introduction

Albania sits in the central portion of the actively convergent boundary between the Eurasian plate and the Adriatic microplate (Fig. 1). As such, compressive tectonics with active shortening in the SW-NE direction and NW-striking thrusts and folds dominate, particularly in the coastal areas. Tectonically, the country is dominated by the presence of the Albanides, the middle section of the Dinarides-Hellenides fold-and-thrust belt that was formed east of the Adriatic Sea since the Late Jurassic as part of the large-scale convergence between Eurasia and Africa (Handy et al., 2019). The regional seismotectonics is controlled by the aforementioned system of NW-SE thrust faulting, but also by two major NE-SW strike-slip structures that control the sedimentary emplacement and tectonic evolution of the Albanides. These tectonic lineaments are the Shkodër-Peja Fault to the north, which separates the Albanides from the Dinarides, and the Vlorë-Elbasan lineament in the south.

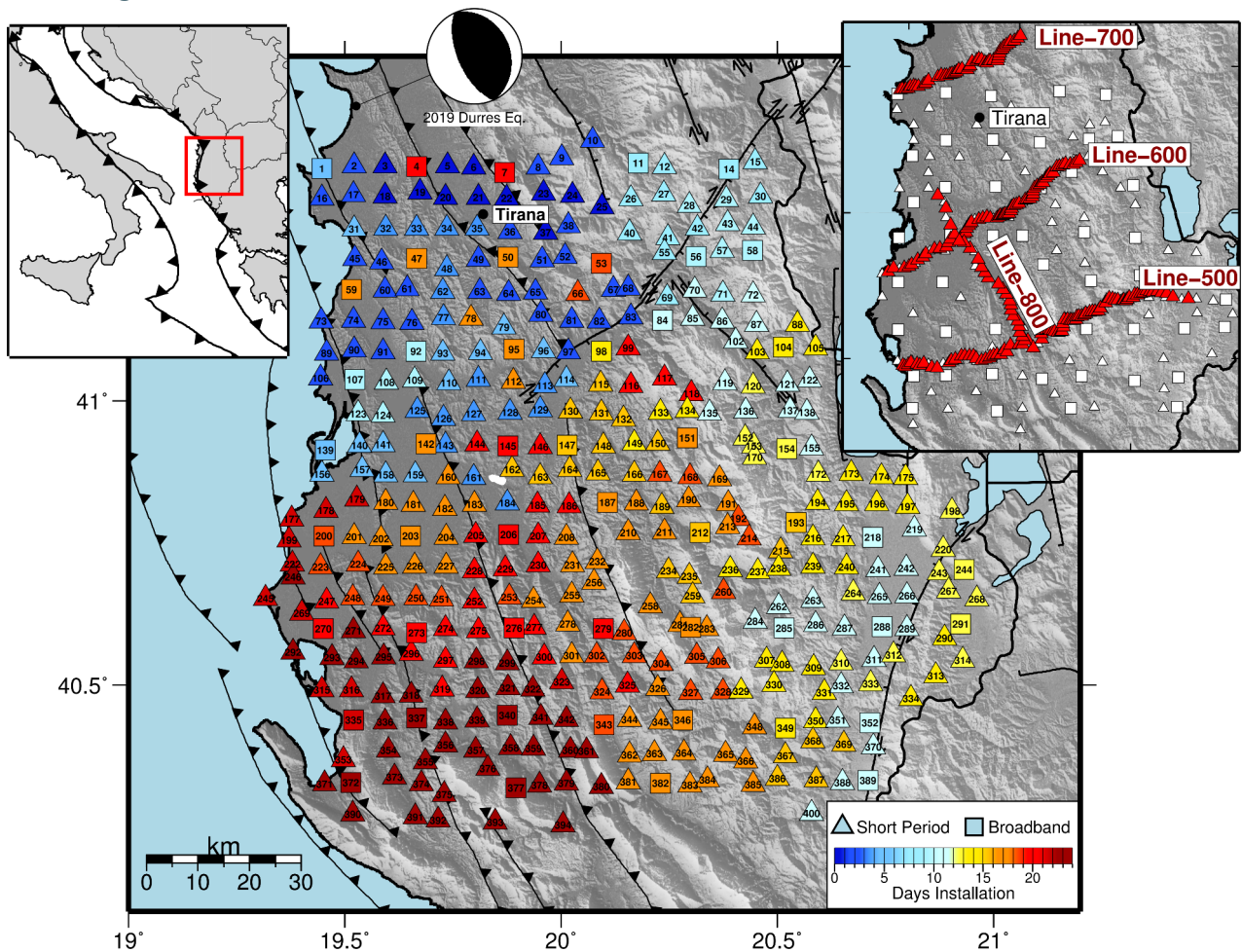


**Figure 1.** Location and first phase (September 2022 to May 2023) network deployment coloured by installation date. Focal mechanism of 2019 Mw=6.4 Durrës earthquake, taken from USGS moment tensor solution. Faults from Styron et al. (2020). Top-right inset: receiver function lines and areal stations remaining throughout the second phase (May 2023 to April 2024).

The Albanides orogen is divided into two tectonic domains: (1) the Internal or Eastern Albanides, composed of metamorphic sequences, particularly Jurassic ophiolites belonging to the suture of the Tethys Ocean, and (2) the External or Western Albanides, characterized by Triassic to Eocene carbonates and Oligocene to Pliocene siliciclastic deposits. Furthermore, a large foredeep basin, the Periadriatic Depression, extends northward from the Vlorë–Elbasan lineament filled with Oligocene to Quaternary deposits. The Albanides division also reflects into the deformation style: while the External Albanides and foredeep are still undergoing shortening with active SW-verging folding and thrusting, the Internal Albanides are currently undergoing extension (Vittori et al., 2021 and references therein).

In our study region, the Moho depth increases from 25–30 km under the Adriatic Sea to 40–50 km under the Albanides axis, whilst the maximum seismogenic depth tends to follow the Moho, with hypocenters mostly in the upper crust down to 20 km depth (Grad et al., 2009; Stipcevic et al., 2020). Small earthquakes ( $M < 4.5$ ) are ubiquitous in Albania, with an  $M_{4.5+}$  earthquake every 1.3 years on average (Aliaj et al., 2010; Muço et al., 2013). Most larger earthquakes ( $M > 5$ ) occur along three well recognized seismic belts: (1) the NW-trending Ionian-Adriatic coastal thrust belt, (2) the N-S trending Peshkopia-Korçë graben fault zone at the East of the country, and (3) the transversal NE-trending Elbasani-Dibra-Tetova normal fault belt that crosses the previous two (Aliaj et al., 2004). Records of historical seismicity show 55 earthquakes with intensity (MSK) larger than VIII up until the 20th century (Aliaj et al., 2010). During the instrumental era (~1900 onwards), 418 events with  $M > 4.5$  occurred up until the year 2000 (Sulstarova et al., 2001). Based on historical records, Aliaj et al. (2004) estimated the maximum earthquake magnitude for the Albanian territory to be 7.25.

Recently, in November 2019, an  $M_w$  6.4 earthquake struck the port town of Durrës with a rupture on a NNW-trending shallowly dipping thrust fault at a depth of 22 km (Teloni et al., 2021). The complete sequence included two  $M > 5$  foreshocks and thousands of aftershocks lasting at least throughout January 2020 (Teloni et al., 2021, Van der Heiden, 2022). The occurrence of this important earthquake and the lack of studies regarding the seismogenesis and velocity structure of the Albanian territory prompted the conception of the project ANTICS (Albanian Tectonics of Continental Subduction).

## 74 2. The ANTICS deployment

75 The large-N ANTICS deployment is an international collaborative effort by the Karlsruhe Institute of Technology  
76 (KIT, Germany), the German Research Center for Geosciences (GFZ, Germany), and the Institute of GeoSciences,  
77 Energy, Water and Environment of the Polytechnic University Tirana (PUT, Albania) that builds on our previous  
78 Durrës aftershock deployment in the region (Schurr et al., 2020). The goal of the ANTICS project is to explore in detail  
79 the seismogenic sources and velocity structure within the Albanian territory, filling in the knowledge gap persistent in  
80 this region. We aim to obtain an accurate local earthquake catalogue and a detailed crustal structure from local  
81 earthquake tomography, full waveform tomography, ambient noise tomography and receiver function analysis.  
82

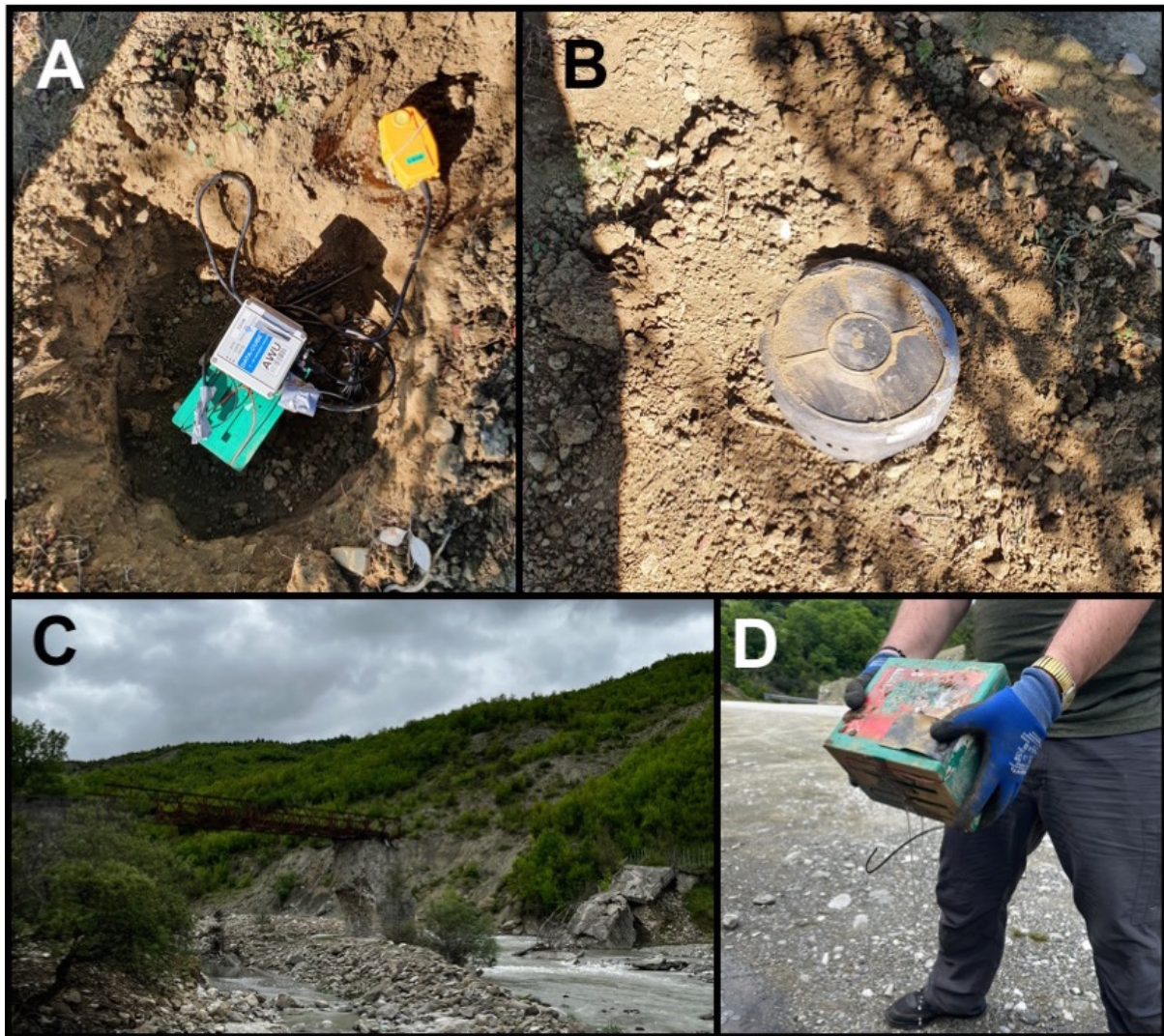
83 The initial network deployment (Phase 1) was carried out by five teams of two people each during a 3-week period  
84 between September 22 and October 13, 2022 (Fig. 1). All instruments were obtained from the GFZ and KIT seismic  
85 pools, with a total of 382 stations installed, including 50 broadband seismometers (Trillium Compacts with flat  
86 response up to 120 s) and 332 3-component geophones (PE-6B with 4.5 Hz corner frequency) recording at a sampling  
87 rate of 100 Hz. The average inter-station spacing was 6 km, with a total covered area of 130×145 km<sup>2</sup>, encompassing a  
88 large part of the Albanian territory including its full W-E extension. The elevation of station sites varied from sea level  
89 to 1740 m, with an average of 533 m.  
90

91 During servicing in May 2023, the network geometry was reconfigured into four profile lines for receiver function  
92 analysis (Phase 2; Fig. 1). Three lines were deployed perpendicular to the orogeny, while the fourth one was deployed  
93 along strike. The nominal inter-station spacing within the lines was 1 km, and because of terrain and logistical  
94 constraints, the installation occurred mostly along roads. A total of 214 geophone stations were moved to these new  
95 sites, while the rest of the original sites, including all 50 broadband stations, were left in place as a backbone areal  
96 distribution. A second service was carried out in September 2023 to download data and exchange batteries, with the  
97 final removal of all stations in April 2024.  
98

99 The setup for each site consisted of a sensor buried at ~50 cm depth, and in a separate hole the data logger, GPS  
100 antenna, battery and cables, semi-buried and covered by an inverted plastic bucket (Fig. 2). Sensors were oriented  
101 according to magnetic north; the magnetic declination in the study region during the deployment period was +5°.  
102 DATA-CUBE 3-channel recorders were used for all stations, with a gain set at 1 for broadband sensors and 16 for short  
103 period sensors. The power source consisted of one (two for broadband stations) non-rechargeable 9v/175Ah dry  
104 alkaline battery, providing an estimated autonomy of ~9 months. Importantly, because the alkaline batteries were of  
105 type metal-air, they had to have access to fresh air and therefore we kept them in a non-waterproof setup allowing  
106 proper ventilation but potentially also allowing the access of water and insects. For stations at elevations above 1000  
107 m where freezing temperatures were expected in winter, we opted for using sealed battery packs of lithium batteries.  
108

109 The most important challenges faced during installation were related to excess of rain and flooding on the roads,  
110 unreliable GPS navigation in remote areas, and mechanical car problems mostly due to the generally poor road  
111 infrastructure. Because of the high density deployment, some of the stations (47) had to be installed outside properties  
112 in open field conditions, though all broadband sensors were installed within properties for safety reasons. During the  
113 second phase, and due to the denser and more strict location of the profiles stations, a total of 110 out of the 214  
114 stations had to be installed outside properties.





116 **Figure 2.** Composite of photos showing setup and deployment. A: initial setup with geophone, battery and Cube  
117 recorder. B: the sensor is buried and covered by soil, and the recorder and battery are covered by an inverted  
118 plastic bucket with small holes on the sides to allow for ventilation. C: Some of the difficulties during fieldwork  
119 included flooded paths and broken road infrastructure. D: flooded battery found during servicing in May 2023.

### 120 **3. Data quality and recovery**

121 Servicing of the entire network was carried out in mid-May 2023. Average data recovery for the first phase was 76%  
122 (median=93%), with 287 (75%) stations recording for 50% of the time or more (Fig. 3). Five stations were unfortunately  
123 stolen and therefore not possible to recover.  
124

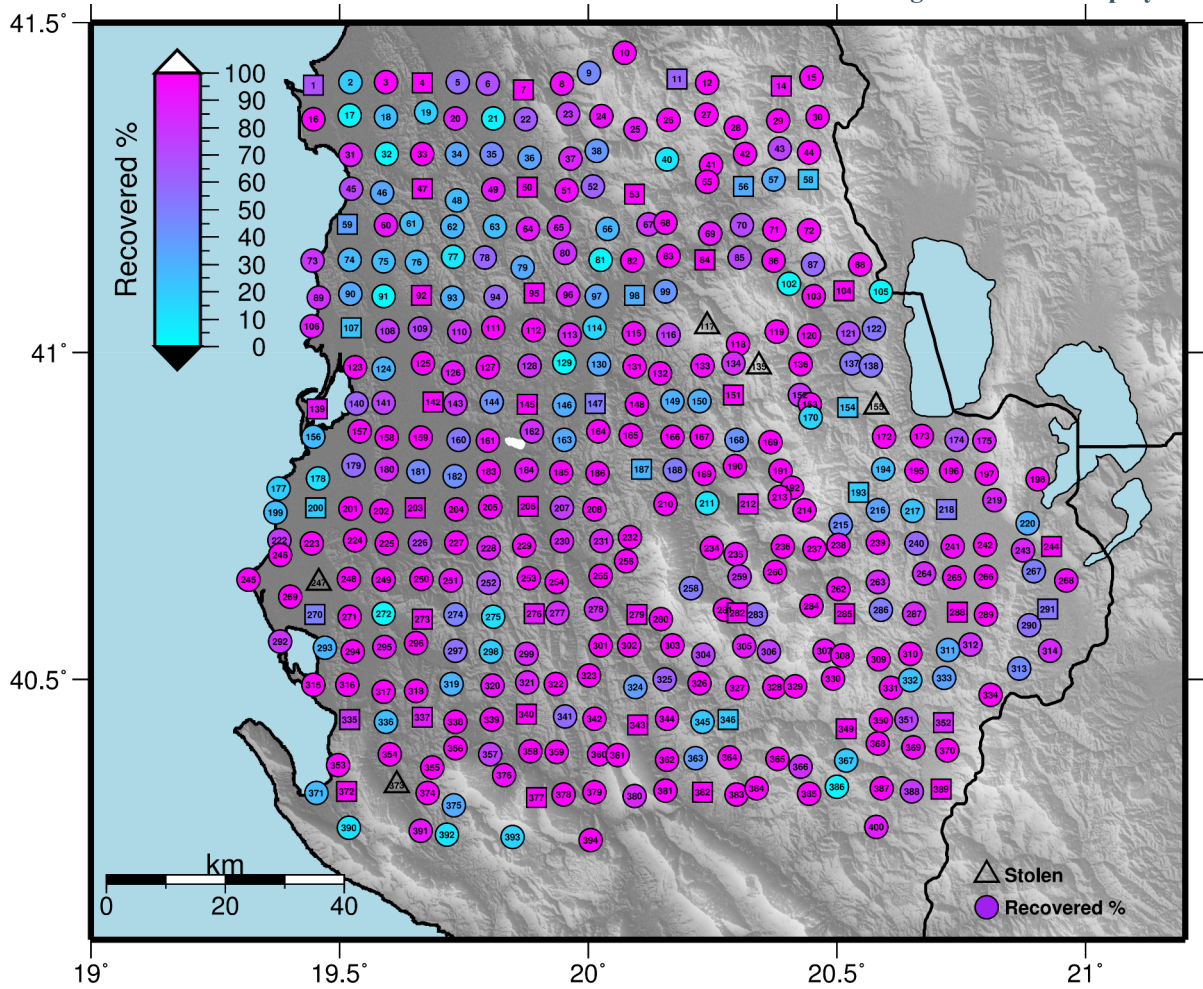


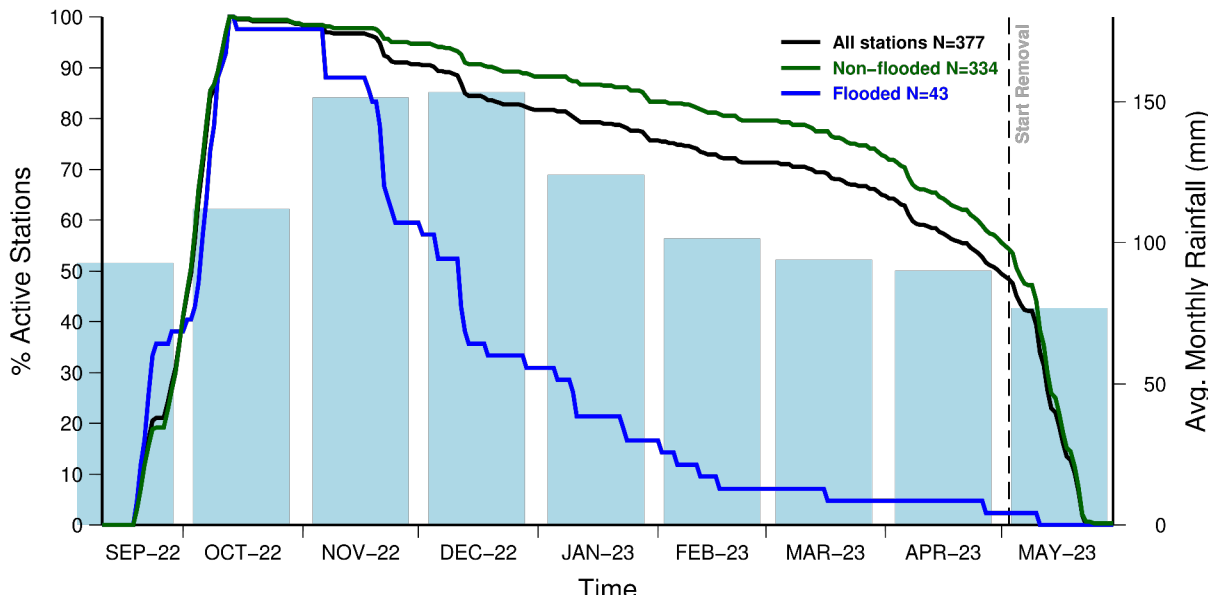
Figure 3. Data recovery during first service, May 2023.

125  
126  
127  
128  
129  
130  
131  
132  
133  
134  
135  
136  
137  
138  
139  
140  
141  
142  
143  
144

The most common cause for incomplete data recovery was battery failure due to flooding. In fact, the average last day recorded for flooded stations was December 18, 2022, which is right after the peak of the rainy season in Albania (Fig. 4). In contrast, the average last recorded day for all stations is March 20, 2023. In total 43 (11%) sites were found with clear signs of flooding, although this is a lower bound given that flooding signs were not always visible or this information was not always collected. Notably, all the flooded sites, except for one, were installed inside a farm or backyard, mostly in clay-rich soils for a lack of a better location. Furthermore, while the average elevation for all stations was 533 m, the average elevation for flooded stations was only 294 m, which again indicates that farming soils at lower elevations had a tendency to flooding, while at higher elevations, rocky soils with better permeability were better suited for our installation. Furthermore, no battery problems were observed due to low temperatures at high altitude. Overall, during the first phase the data suggest that once a given station survived the rainy period, chances are that it recorded until the first servicing in May 2023 or shortly before that.

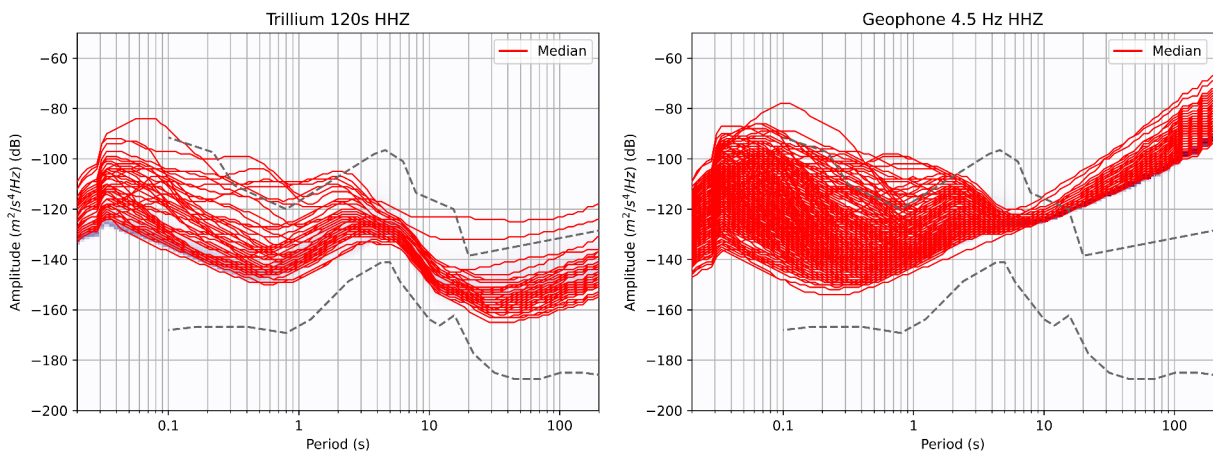
On the other hand, many of the batteries exchanged during the second service in September 2023 run out prematurely, resulting in many stations stopping acquisition in December 2023, showing no clear correlation with site conditions. We suspect that this problem was due to a bad batch of batteries with reduced capacity, although they were freshly ordered before servicing and did not show any anomalies in pre-deployment voltage checks.





147 **Figure 4.** Correlation between active stations and historical rainfall as a function of time. A steep fall in active  
 148 stations coincides with periods of heavy rainfall and therefore potential site flooding. Precipitation data from  
 149 <https://climateknowledgeportal.worldbank.org/country/albania/climate-data-historical> (last visited 12 October  
 150 2024).  
 151

152 Fig. 5 shows the noise levels for all broadband and short-period stations during the first phase (September 2022 to  
 153 May 2023) as Probabilistic Power Spectral Density (PPSD) median curves of their vertical component (e.g. Custodio et  
 154 al., 2014). In general, broadband stations noise levels are below the high noise model, except for five stations that  
 155 show higher noise levels at periods between 0.2 and 2 s. Geophones show a similar distribution, with higher noise  
 156 levels between 0.2-2 s, and instrumental self-noise dominating for periods longer than about 5 s. The secondary  
 157 microseismic noise peak occurs at 2-3 s, at significantly shorter period than the global average. In general, stations  
 158 installed outside properties are considerably quieter than stations inside properties (Sup. Fig. 1), but a few free-field  
 159 stations installed outside properties still present high levels of noise.  
 160



162 **Figure 5.** PPSD curves of vertical acceleration noise median for broadband (left) and short period (right) stations,  
 163 corresponding to the first phase of the project (September 2022 – May 2023).  
 164  
 165  
 166  
 167  
 168

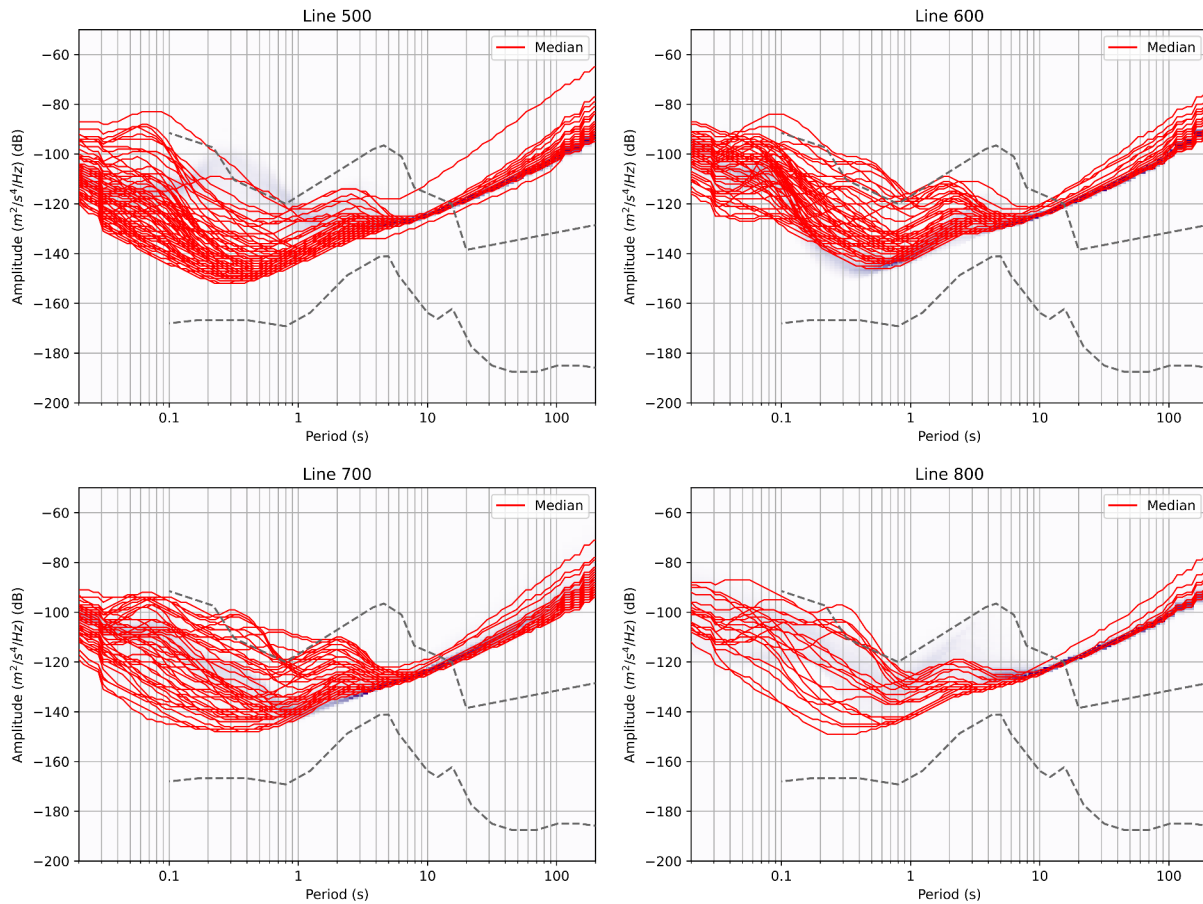
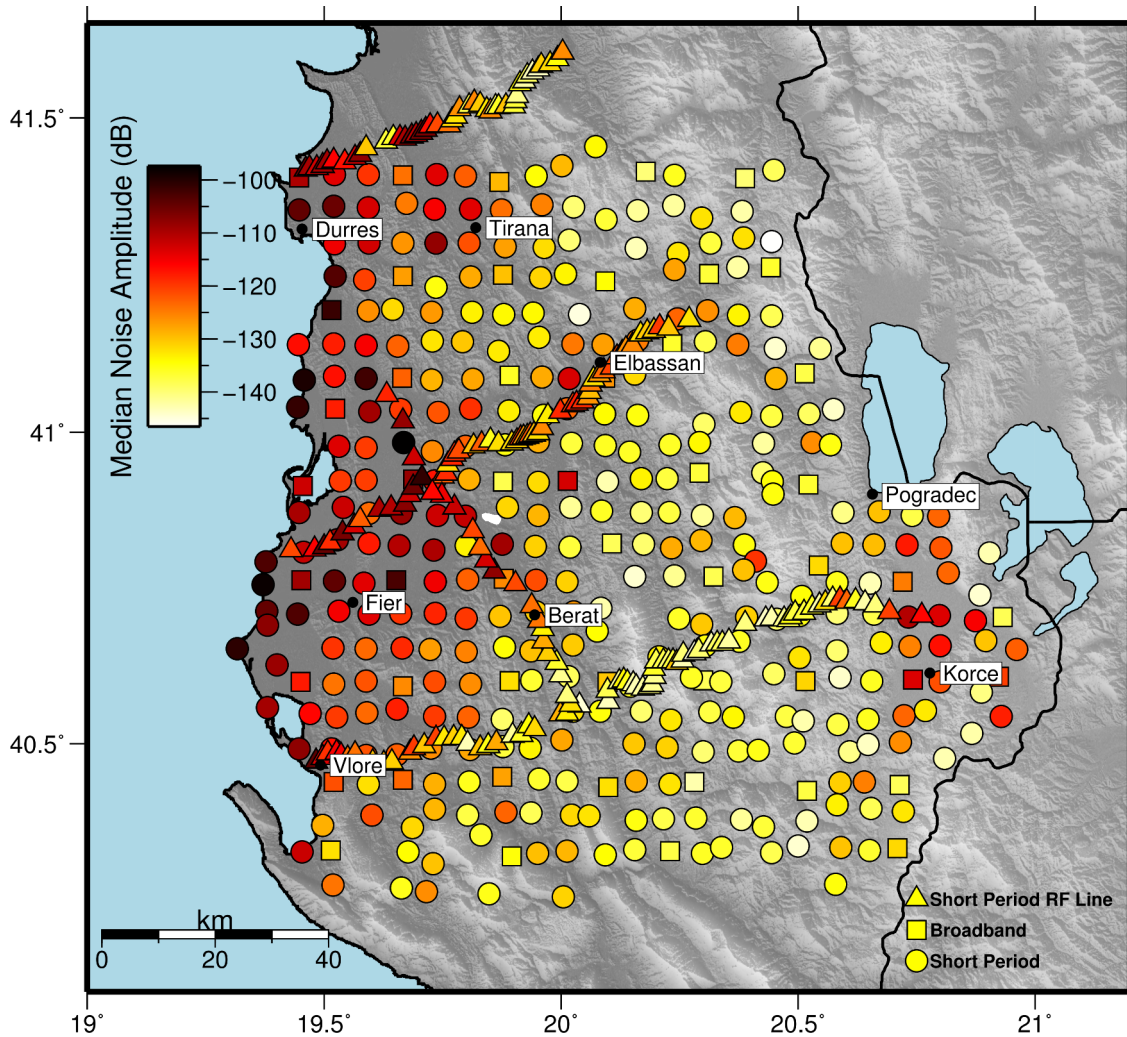


**Figure 6. PPSD curves of vertical acceleration noise median for short period stations in receiver function lines, corresponding to the second phase of the project (May 2023 to April 2024).**

170  
 171  
 172  
 173 Similarly, Fig. 6 shows PPSD noise median curves for the short-period stations included in the four RF lines during  
 174 the second phase (May 2023 to April 2024). In general, line-500 seems to be the quietest one, with the other three lines  
 175 showing a more diverse range of noise amplitudes, some of them above the high noise model. Notably, line-500 was  
 176 deployed in the more remote and mountainous southern area, while the other 3 lines, particularly lines 600 and 800,  
 177 were deployed along important roads with nearby populated centres. This can be better seen in Fig. 7, which shows in  
 178 map view the average median noise amplitude for all stations in the period band 0.05 to 2 seconds. There appears to be  
 179 a clear trend from northwestern ‘noisier’ stations to southeastern ‘quieter’ stations. This can be explained as the NW  
 180 contains sedimentary basins in low elevation lands close to the sea, with nearby important populated centres. On the  
 181 other hand, as we move to the SE we gain in elevation, depart from the sea and the population is more scarcely  
 182 distributed. A clear exemption to this rule are the noisier stations located nearby Korçë, which can be justified  
 183 precisely by the presence of this city, the largest in eastern Albania, and the emplacement of Quaternary deposits in  
 184 the valley. On a closer examination, a more direct first order anti-correlation seems to exist between noise amplitude  
 185 and terrain slope. For example, the middle section of line-700 contains anomalously noisier stations in a flatter valley  
 186 area in comparison with the surrounding stations in areas of greater slope. This also holds true for the noisier stations  
 187 north of Korçë. Certainly flatter areas are more populated and bisected by more transited roads as opposite to rough  
 188 terrain where more scarce population is expected and therefore lower anthropogenic noise levels. Also, flatter areas  
 189 are generally covered by a thicker sedimentary layer that amplifies the seismic noise, whilst rougher terrain often  
 190 correlates with the outcrop of bed rock. In fact, the distribution of noisier stations (orange and red colours) matches  
 191 well that of the Neogene-Quaternary deposits (e.g. Teloni et al., 2021). Still, it could be interesting for future  
 192 deployments to consider an easily available parameter such as elevation or terrain slope as a first order indication of  
 193 expected noise level (Sup. Fig. 4), in addition to other more obvious but harder to obtain parameters such as  
 194 population density, road traffic or geology (e.g. Wald and Allen, 2007).





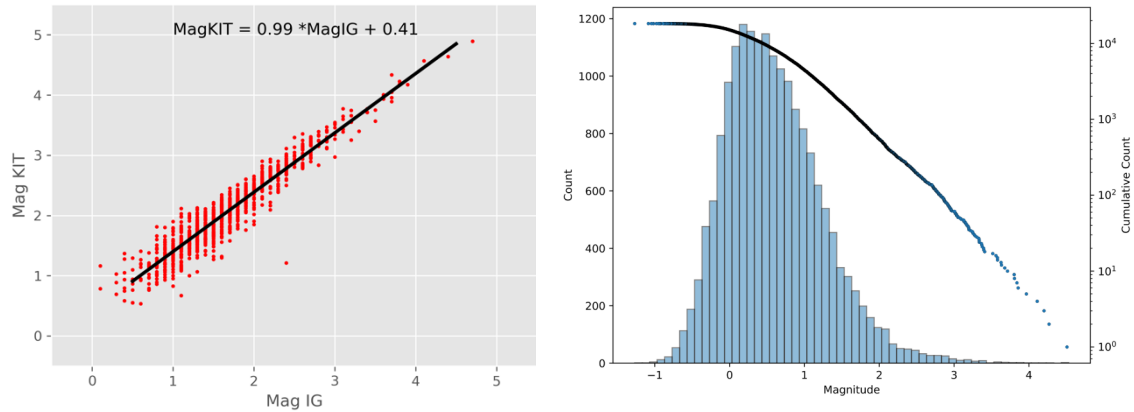
196 **Figure 7.** Average of median vertical acceleration noise amplitude per station for frequency range 0.05 to 2 s (0.5-20  
 197 Hz). Important cities indicated by black dots.

#### 198 **4. Preliminary Earthquake Catalogue**

199 The continuous waveforms collected from September 2022 to May 2023 were processed with an AI-based  
 200 automatic picker PhaseNet (Zhu et al., 2019), obtaining 38.4 M picks of which 20.8 M are P phases and 16.6 M are S  
 201 phases. These picks were then associated into events using the AI-based HEX algorithm (Woollam et al., 2020,  
 202 2022). For this step we used a selection of 95 homogeneously distributed stations given that the use of all 382  
 203 densely placed stations produced an excess of false detections. Nearly 18k events were detected with at least 8 P-  
 204 and 3 S-phases, associating 1.93 M picks. All 18k events were then relocated using a 1-D velocity model (Dushi and  
 205 Havskov, 2023) and the NonLinLoc algorithm (Lomax, 2009) which provides a full probabilistic density function for  
 206 each hypocentral location.

207  
 208 Local magnitudes were calculated using maximum peak-to-peak amplitudes of the S-phase on the horizontal  
 209 components and an empirical relationship for the region (Muço and Minga, 1991). We then benchmarked and  
 210 corrected our estimations with 1028 common events from the manually picked local earthquake catalogue of the  
 211 IGEO-PUT (Bulletin of the Albanian Seismic Network), obtaining a simple linear trend with a slope of nearly 1 but a  
 212 positive bias of 0.4 magnitude units with respect to the local catalogue (Fig 8). After correcting for this bias, our  
 213 final magnitudes range from -1.0 to 4.5, with a magnitude of completeness ( $M_c$ ) of  $\sim 1.5$ . Five earthquakes  $M_L \geq 4.0$   
 214 occurred during the deployment period, the largest of them associated to the January 2023 Klos sequence.  
 215

216  
217  
218  
219



221 **Figure 8. Left: linear relationship between initial magnitudes from this work and from the IG-PUT local catalogue.**  
222 **Right: frequency-magnitude distribution of final magnitudes.**

223

224

225

226

227

228

229

230

231

232

233

234

235

236

237

238

239

240

241

242

243

244

245

246

247

248

249

The temporal evolution of seismicity (Fig. 9) shows an average daily rate of 70 earthquakes per day, while two maxima of 700-800 events per day are observed associated to the Klos and Erseke sequences, respectively. Figure 10 shows a selection of ~10800 events with at least 10 P, 4 S phases, and location uncertainties less than 5 km. The seismicity seems to be distributed in clusters and along known major structures. Events occur down to 30 km depth, notably with a decrease of the seismogenic depth from 30 to 20 km depth from North to South. Noteworthy is the fact that no seismicity is observed in the epicentral area of the 2016 Durrës earthquake, which would indicate a complete return to background seismicity levels following the aftershock period of that earthquake (Van der Heiden, 2021).

Two earthquake clusters were particularly productive during our study period: to the north, the Klos sequence occurred in January 2023, and to the south, the Erseke sequence, occurred in March 2023. The Klos sequence seems to start in January 13 with an  $M_L$  3.0 earthquake, which elevated the daily rate of seismicity to nearly 400 events per day in the nearby area (Sup. Fig. 6). The following next two days the seismicity rate decayed until the evening of January 15 when the  $M_L$  4.5 mainshock occurred, which again elevated the daily rate of seismicity to above 700 events per day. The whole sequence is confined to depths 5-20 km depth, with all hypocenters  $M_L \geq 3.0$  near the bottom of the seismogenic layer, ranging 15-20 km depth. Spatially, the seismicity seems to be associated to a large normal fault NW-striking. This is corroborated by our moment tensor solution (e.g. Lindner, 2023) for the Klos mainshock, which indicates oblique normal faulting with a similar strike (Fig. 10).

The Erseke sequence started with an  $M_L$  4.3 mainshock on the 23 of March 2023, which elevated the daily rate of seismicity to almost 800 events per day in the nearby area (Sup Fig. 7). For the next ten days, the seismicity rate decays, although some bursts of seismicity are seen on March 24 and 26 as secondary aftershock sequences of large aftershocks. The seismicity occurs mostly between 3 to 17 km depth, with the mainshock hypocenter located at 17 km. Spatially, the sequence is associated to a large oblique normal fault striking NNE (Fig. 10).

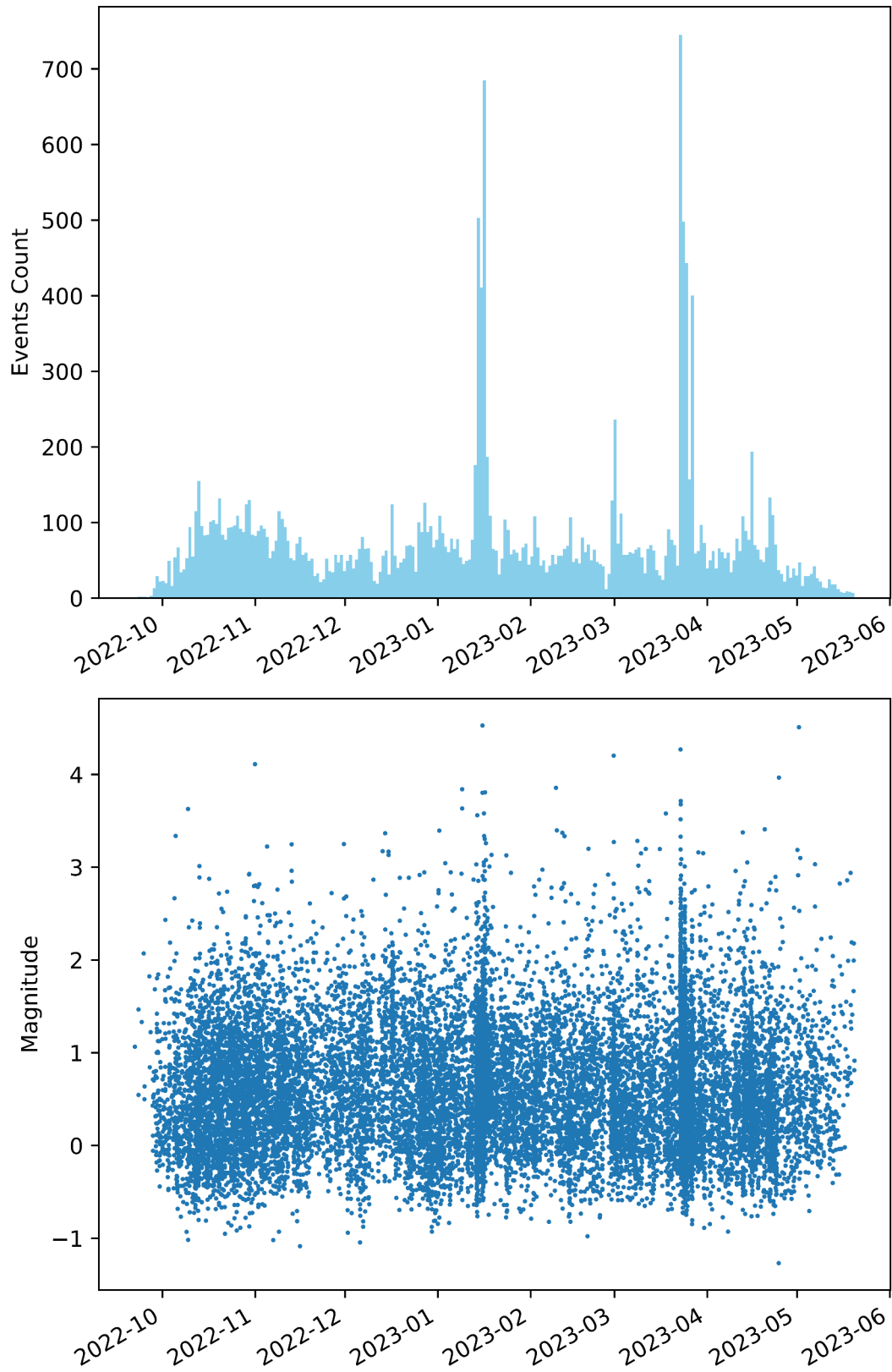
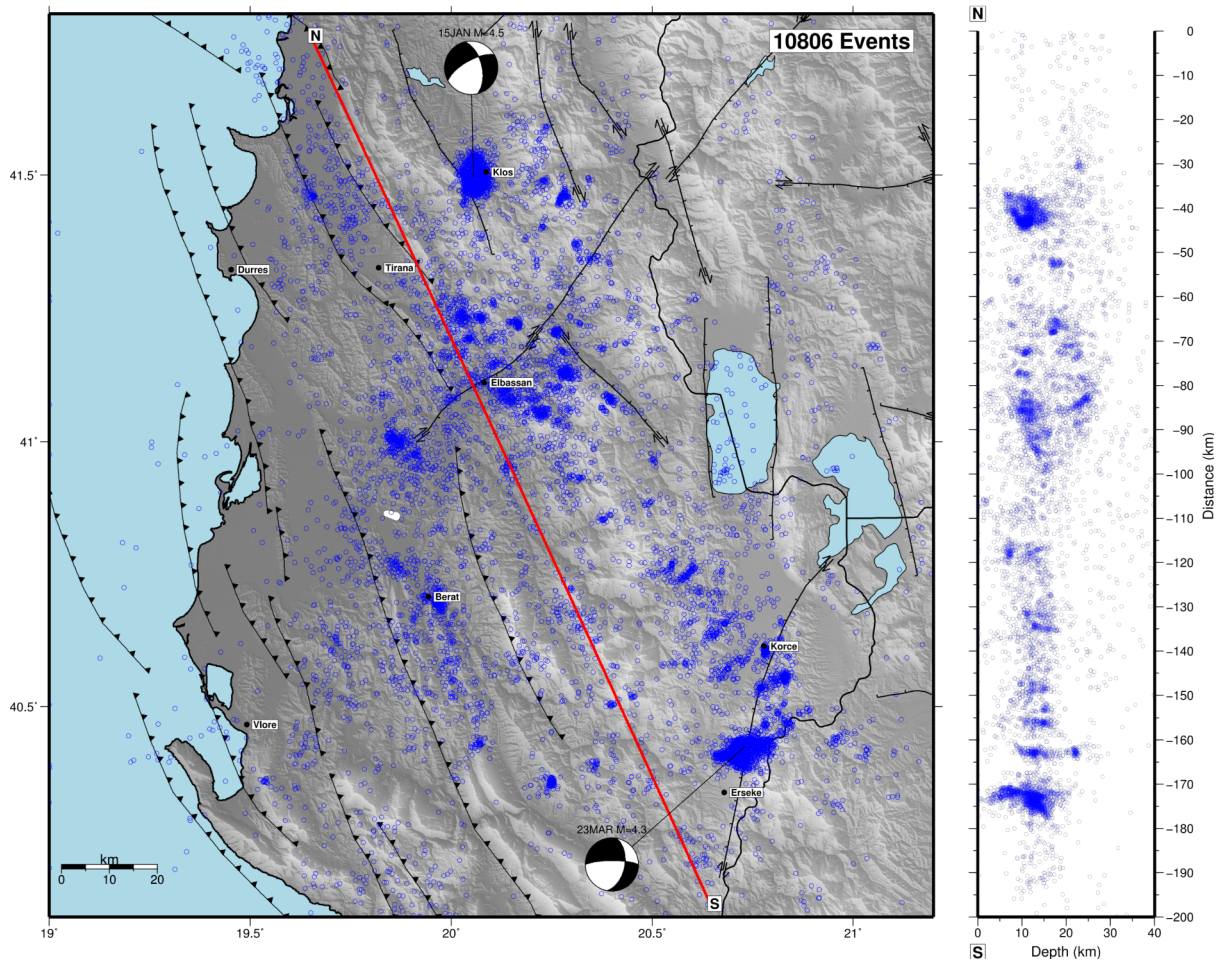


Figure 9. Temporal evolution of seismicity as daily rate (upper panel) and magnitude occurrence (lower panel).





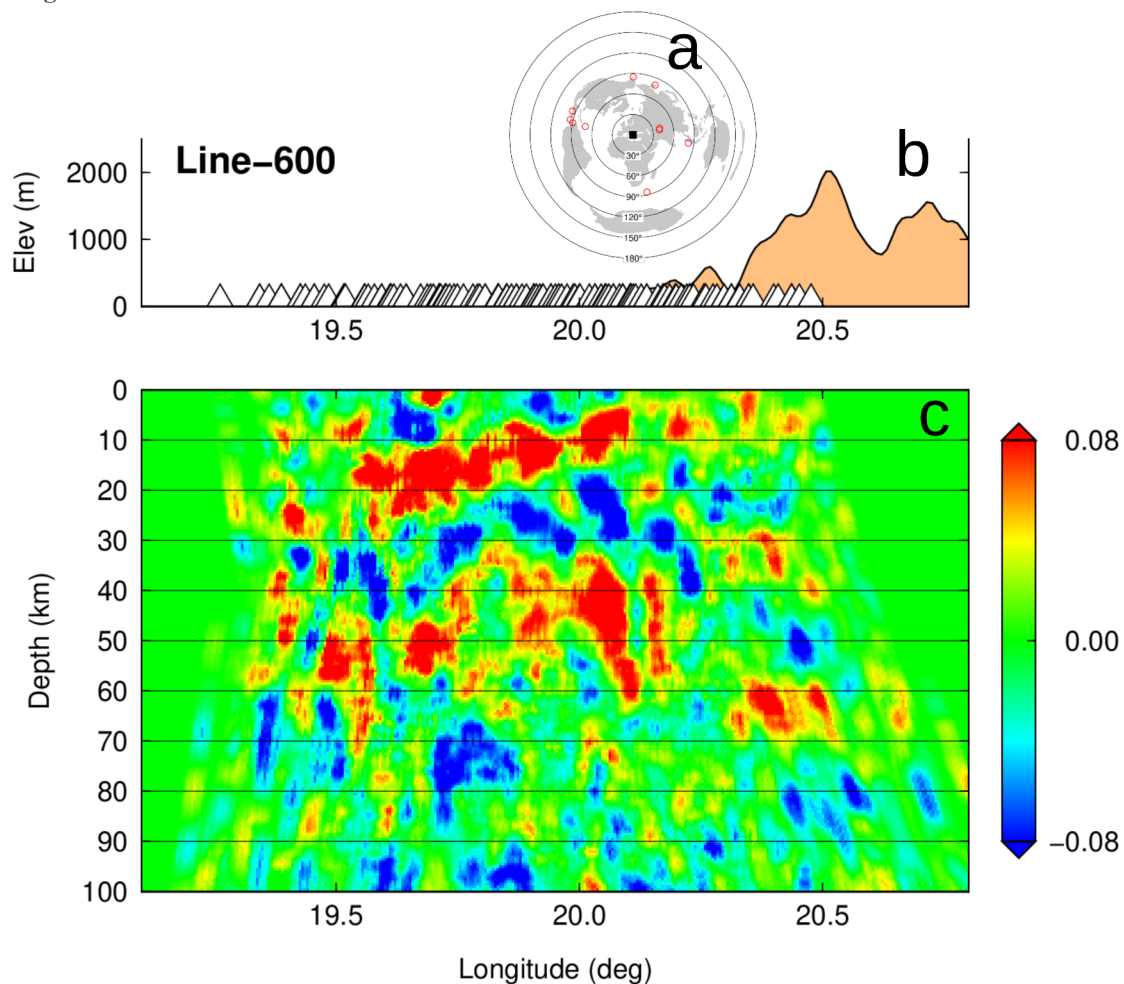
253 **Figure 10. Seismicity map and NW-SE depth section.**

## 254 **5. Preliminary receiver function analysis**

255 Passive-source seismic imaging using the receiver function (RF) method is commonly used to study the  
 256 structure in the crust and upper mantle. Conventional RFs are computed using broadband data and are usually  
 257 stacked over a large number of teleseismic events to enhance the signal/noise ratio. In recent years the use of short-  
 258 period stations has been greatly increased and has proven successful in extracting RFs (Yuan et al. 1997; Ward et al.  
 259 2017). Here we show that it is feasible to apply the RF analysis to the ANTICS large-N experiment.

260  
 261 Fig. 11 is a preliminary Common-Conversion-Point (CCP) stacked RF cross section along one of the linear  
 262 profiles with densely spaced stations (Line-600). Ten events with magnitudes greater than 6.5 occurring between  
 263 October 2022 and July 2023 are used, five in the first phase and five in the second phase of the experiment (Fig. 11a).  
 264 The majority of stations are short-period geophones with a natural frequency of 4.5 Hz, which is outside the normal  
 265 teleseismic frequency range usually of 0.1-1 Hz. Therefore, the instrument response has been deconvolved from  
 266 the raw data to enhance teleseismic signals and simulate broadband records. Three-component data are visually  
 267 inspected and processed with the RF analysis, involving component rotation and deconvolution. RF cross sections  
 268 were constructed along the four linear profiles with a swath width of 20 km. Figure 11c is an example of Line-600,  
 269 along with some conspicuous crustal interfaces. The profile crosses a prominent sedimentary basin to the west and  
 270 a mountainous area to the east. The interface at shallow depths down to 20 km may represent the crystalline  
 271 basement that dips to the west. We note that indicated depths are biased downward as we did not correct for slower  
 272 seismic velocities in the sedimentary layer in this preliminary processing. The multiples of the basement may  
 273 dominate the 40-60 km depth range. There appears to be evidence of the Adriatic Moho that dips to the east to a  
 274 depth of 65 km. Further analysis with the complete dataset is needed to verify these preliminary observations.





275 **Figure 11.** a) Distribution of used teleseismic events (10); b) Elevation profile and stations along Line-600; c)  
 276 Preliminary RF cross section showing some prominent crustal converters. Red/blue colors indicate  
 277 positive/negative converted phases, representing downward velocity increase/decrease.

## 278 6. Lessons learned and outlook

279 Given the density and large number of installed stations, and despite the adverse road and meteorological  
 280 conditions, the ANTICS deployment was swiftly and successfully achieved. In a period of three weeks during  
 281 September-October 2022, we managed to install 382 seismic stations in a wide range of terrain and elevation  
 282 conditions. Considering the installation and subsequent servicing, we gathered the following valuable lessons:

283 (a) Meteorological and seasonal conditions should be taken into account for the deployment schedule to  
 284 reduce the likelihood of data loss due to intense rain periods. In that sense, when a rainy period lies within the  
 285 deployment period, a service run checking on the stations should be organised as soon as possible thereafter.

286 (b) It is important to consider soil permeability of the sites, in order to avoid flooding due to poor permeability.  
 287 A good rule of thumb is to avoid clay-rich soils.

288 (c) Metal-air batteries are a good option for temporary deployments such as ours, but attention should be put  
 289 into not burying too much the batteries and always keeping the upper half of it above surface to avoid penetration  
 290 and accumulation of water. This of course has to be balanced with the fact that the equipment should be concealed  
 291 to avoid robbery and damage when installing outside properties.

292 (d) Once a station continued working during the rainy season, chance is that it will record until the end. In that  
 293 sense, there were no problems inherent to battery durability, at least during the first phase of our experiment.

294 (e) Having said that, battery problems did occur after the second service likely due to a bad batch of batteries  
 295 with reduced capacity. Therefore, randomly checking batteries capacity before installation and, if possible, re-  
 296 visiting a subset of sites after servicing is recommended in order to detect probable systematic power problems  
 297 early on.

298

299

300

301 **Data availability statement.** The ANTICS dataset (<https://geofon.gfz-potsdam.de/doi/network/X3/2022>) will be openly  
302 available at the GEOFON web service from May 2028 (DOI:).

303  
304 **Acknowledgements.** We thank the Geophysical Instrument Pool Potsdam (GIPP) for loaning the seismic equipment (loan  
305 202214). We also acknowledge the support and funding from Karlsruhe Institute of Technology. We are indebted to all  
306 the Albanian landowners that allowed us to install stations in their properties and looked after them during the project.  
307 We also thank all the personnel involved in the installation and servicing of stations, and related logistics: Felix  
308 Bögelspacher, Kleo Allka, Rrezart Bozo, Benedikt Braszus, Gazmir Çela, Arnaud Dalsuc, Marson Dyrmishi, Almir Gjata,  
309 Altin Gjonaj, Olgert Gjuzi, Hamdi Hasa, Susanne Hemmleb, Rune Helk, Laura Hillmann, Damiano Koxhaj, Agur Lybeshari,  
310 Peter Makus, Lenny Mejía, Leon Merkel, Ardian Mile, Ylber Muceku, Dionald Muçollari, Naim Nazeri, Vilson Ndoni, Klei  
311 Prifti, Arben Radheshi, Indrit Rexhepi, Susann Richter, Gjon Rota, Zenel Rroko, Christoph Sens-Schönfelder, Gjergji Stoja,  
312 Marsel Tamo, Anila Xhahysa and Thomas Zieke.

## 313 References

- 314 Aliaj, Sh., Adams, J., Halchuk, S., Sulstaorva, E., Peci, V., Muço, B. 2004. Probabilistic hazard maps for Albania. 13th  
315 WCEE Vancouver, Canada, August 1-6, 2004, Paper No 2469.
- 316 Aliaj, S., Kociu, S., Muço, B. & Sulstarova, E., 2010. Seismicity, Seismotectonics and Seismic Hazard Assessment in  
317 Albania, Academy of Sciences of Albania, pp. 98.
- 318 Bulletin of the Albanian Seismic Network. Monthly bulletin of seismology. Country: Albania. Medium: Online,  
319 ISSN:2664-410X. [https://www.geo.edu.al/Services/Department\\_of\\_Seismology/](https://www.geo.edu.al/Services/Department_of_Seismology/)
- 320 Custódio, S., Dias, N.A., Caldeira, B., Carrilho, F., Carvalho, S., Corela, C., Díaz, J., Narciso, J., Madureira, G., Matias,  
321 L. and Haberland, C., 2014. Ambient noise recorded by a dense broadband seismic deployment in western  
322 Iberia. *Bulletin of the Seismological Society of America*, 104(6), pp.2985-3007.
- 323 Dushi, E.D. and Havskov, J., 2023. 1D crustal structure of Albania region. *Annals of Geophysics*, 66(1), pp.SE103-  
324 SE103.
- 325 Grad, M., Tiira, T. and ESC Working Group, 2009. The Moho depth map of the European Plate. *Geophysical journal*  
326 *international*, 176(1), pp.279-292.
- 327 Handy, M.R., Giese, J., Schmid, S.M., Pleuger, J., Spakman, W., Onuzi, K. and Ustaszewski, K., 2019. Coupled crust  
328 mantle response to slab tearing, bending, and rollback along the Dinaride-Hellenide orogen. *Tectonics*, 38(8),  
329 pp.2803-2828.
- 330 Lindner, M., Rietbrock, A., Bie, L., Goes, S., Collier, J., Rychert, C., Harmon, N., Hicks, S.P., Henstock, T. and VoiLA  
331 Working Group, 2023. Bayesian regional moment tensor from ocean bottom seismograms recorded in the  
332 Lesser Antilles: Implications for regional stress field. *Geophysical Journal International*, 233(2), pp.1036-  
333 1054.
- 334 Lomax, A., Virieux, J., Volant, P. and Berge-Thierry, C., 2000. Probabilistic earthquake location in 3D and layered  
335 models: Introduction of a Metropolis-Gibbs method and comparison with linear locations. *Advances in*  
336 *seismic event location*, pp.101-134.
- 337 Muço, B., 2013. Probabilistic seismic hazard assessment in Albania. *Italian Journal of Geosciences* 132(2): 194–202.  
338 <https://doi.org/10.3301/ijg.2012.33>.
- 339 NASA JPL. 2013. NASA Shuttle Radar Topography Mission Global 1 arc second [Data set]. NASA EOSDIS Land  
340 Processes Distributed Active Archive Center. Accessed 2024-11-19 from  
341 <https://doi.org/10.5067/MEaSURES/SRTM/SRTMGL1.003>
- 342 Schurr, B., Dushi, E., Rietbrock, A., Duni, L. 2020. AlbACa Albanian Earthquake Aftershock Campaign. GFZ Data  
343 Services. Other/Seismic Network. doi:10.14470/4X7564679396.
- 344 Stipčević, J., Herak, M., Molinari, I., Dasović, I., Tkalčić, H. and Gosar, A., 2020. Crustal thickness beneath the  
345 Dinarides and surrounding areas from receiver functions. *Tectonics*, 39(3), p.e2019TC005872.
- 346 Styron, Richard, and Marco Pagani. 2020. The GEM Global Active Faults Database. *Earthquake Spectra*, vol. 36, pp.  
347 160–180, doi:10.1177/8755293020944182.
- 348 Sulstarova, E., Aliaj, Sh. 2001. Seismic Hazard Assessment in Albania. *Albania Journal Of Natural & Technical*  
349 *Sciences* 10: 89-100.
- 350 Teloni, S., Invernizzi, C., Mazzoli, S., Pierantoni, P.P. and Spina, V., 2021. Seismogenic fault system of the Mw 6.4  
351 November 2019 Albania earthquake: New insights into the structural architecture and active tectonic setting

- 352 **Hans Agurto-Detzel et al.**  
of the outer Albanides. *Journal of the Geological Society*, 178(2), pp.jgs2020-193.
- 353 Van der Heiden, V. 2021. Analysis of the 2019 *M<sub>w</sub>* 6.4 Albania aftershock sequence: An updated velocity model  
354 using AI-based solutions, Master's thesis, Karlsruhe Institute of Technology, Geophysical Institute.
- 355 Vittori, E., Blumetti, A.M., Comerci, V., Di Manna, P., Piccardi, L., Gega, D. and Hoxha, I., 2021. Geological effects  
356 and tectonic environment of the 26 November 2019, *M<sub>w</sub>* 6.4 Durrës earthquake (Albania). *Geophysical*  
357 *Journal International*, 225(2), pp.1174-1191.
- 358 Wald, D.J. and Allen, T.I., 2007. Topographic slope as a proxy for seismic site conditions and amplification. *Bulletin*  
359 *of the Seismological Society of America*, 97(5), pp.1379-1395.
- 360 Ward, K. M., & Lin, F. C., 2017. On the viability of using autonomous three-component nodal geophones to  
361 calculate teleseismic *P<sub>s</sub>* receiver functions with an application to Old Faithful, Yellowstone. *Seismological*  
362 *Research Letters*, 88(5), 1268-1278.
- 363 Woollam, J., Rietbrock, A., Leitloff, J. and Hinz, S., 2020. Hex: Hyperbolic event extractor, a seismic phase  
364 associator for highly active seismic regions. *Seismological Society of America*, 91(5), pp.2769-2778.
- 365 Woollam, J., Münchmeyer, J., Tilmann, F., Rietbrock, A., Lange, D., Bornstein, T., Diehl, T., Giunchi, C., Haslinger,  
366 F., Jozinović, D. and Michelini, A., 2022a. SeisBench—A toolbox for machine learning in seismology.  
367 *Seismological Society of America*, 93(3), pp.1695-1709.
- 368 Yuan, X., J. Ni, R. Kind, J. Mechie, and E. Sandvol., 1997. Lithospheric and upper mantle structure of southern Tibet  
369 from a seismological passive source experiment, *J. Geophys. Res.* 102, no. B12, 27,491–27,500.
- 370 Zhu, W. and Beroza, G.C., 2019. PhaseNet: a deep-neural-network-based seismic arrival-time picking method.  
371 *Geophysical Journal International*, 216(1), pp.261-273.
- 372  
373  
374

\*CORRESPONDING AUTHOR: Hans AGURTO-DETZEL,

Geophysical Institute, Karlsruhe Institute of Technology, Karlsruhe, Germany

e-mail: hans.detzel@kit.edu

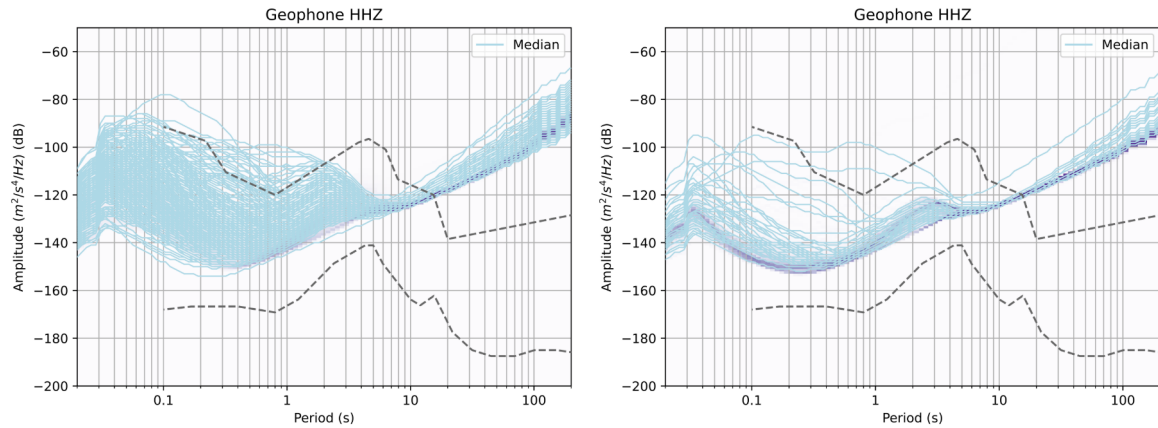
© 2022 the Author(s). All rights reserved. Open Access.

This article is licensed under a Creative Commons Attribution 3.0 International

## Supplementary Material

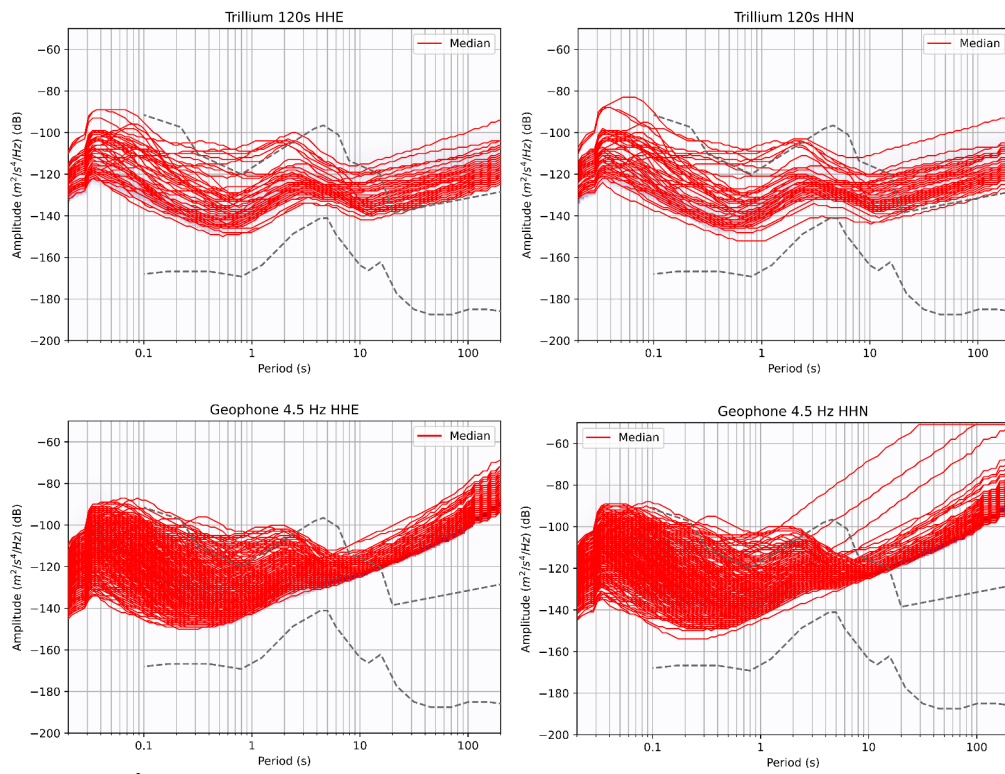
### The ANTICS Large-N Seismic Deployment in Albania

Hans Agurto-Detzel, Andreas Rietbrock, Frederik Tilmann, Edmond Dushi, Michael Frietsch, Ben Heit, Sofia-Katerina Kufner, Mike Lindner, Besian Rama, Bernd Schurr, Xiaohui Yuan.

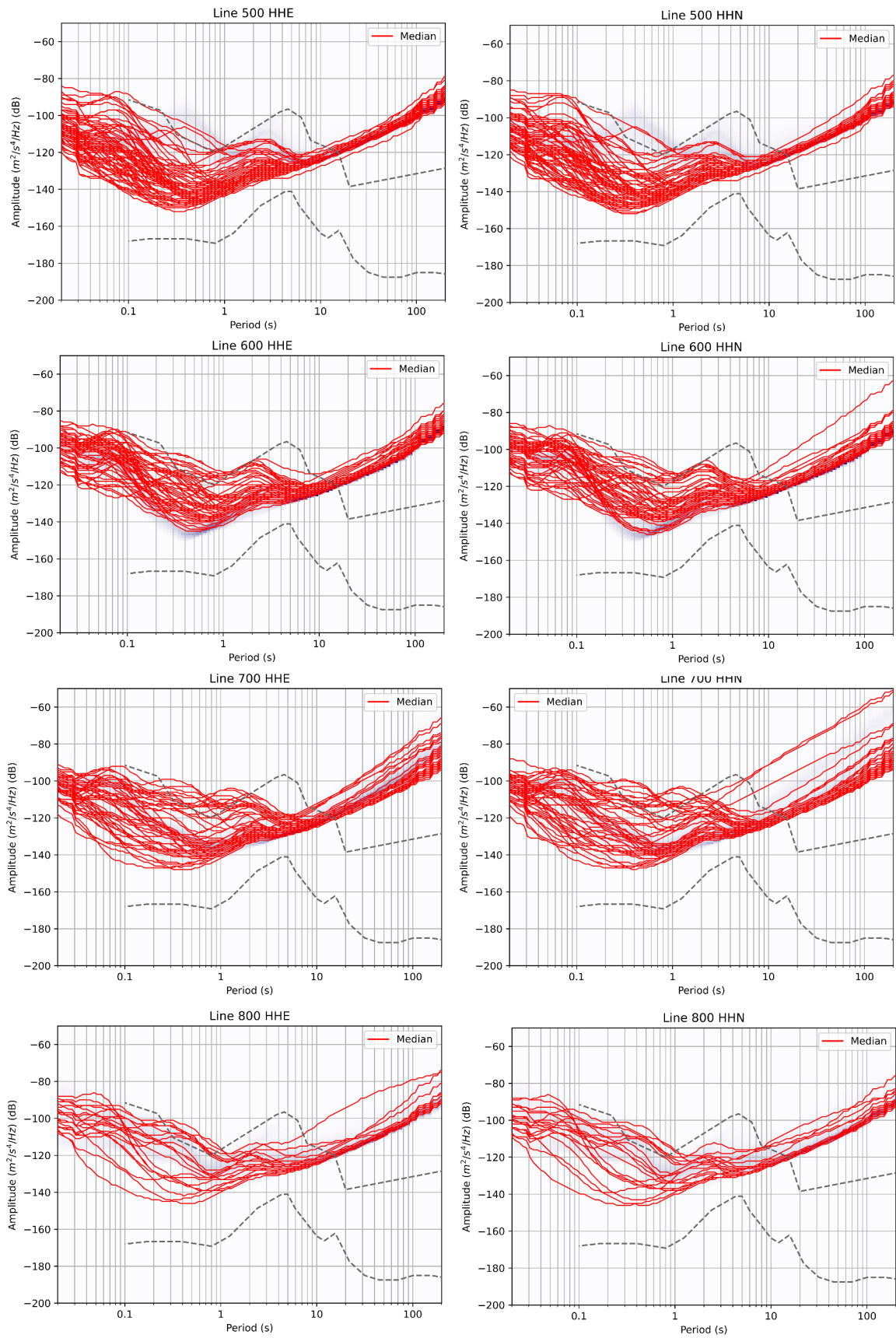


**Supplementary Figure 1.** PSD curves of vertical acceleration noise median for geophones installed inside properties (left) and outside properties (right).

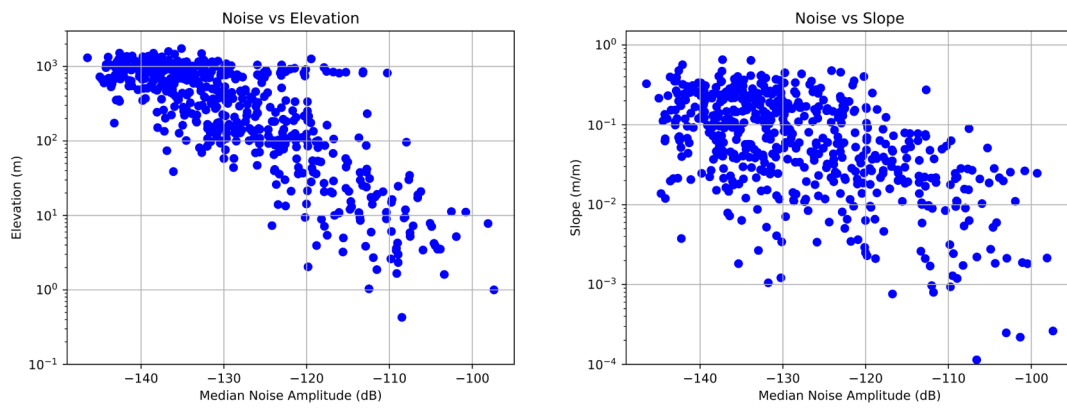




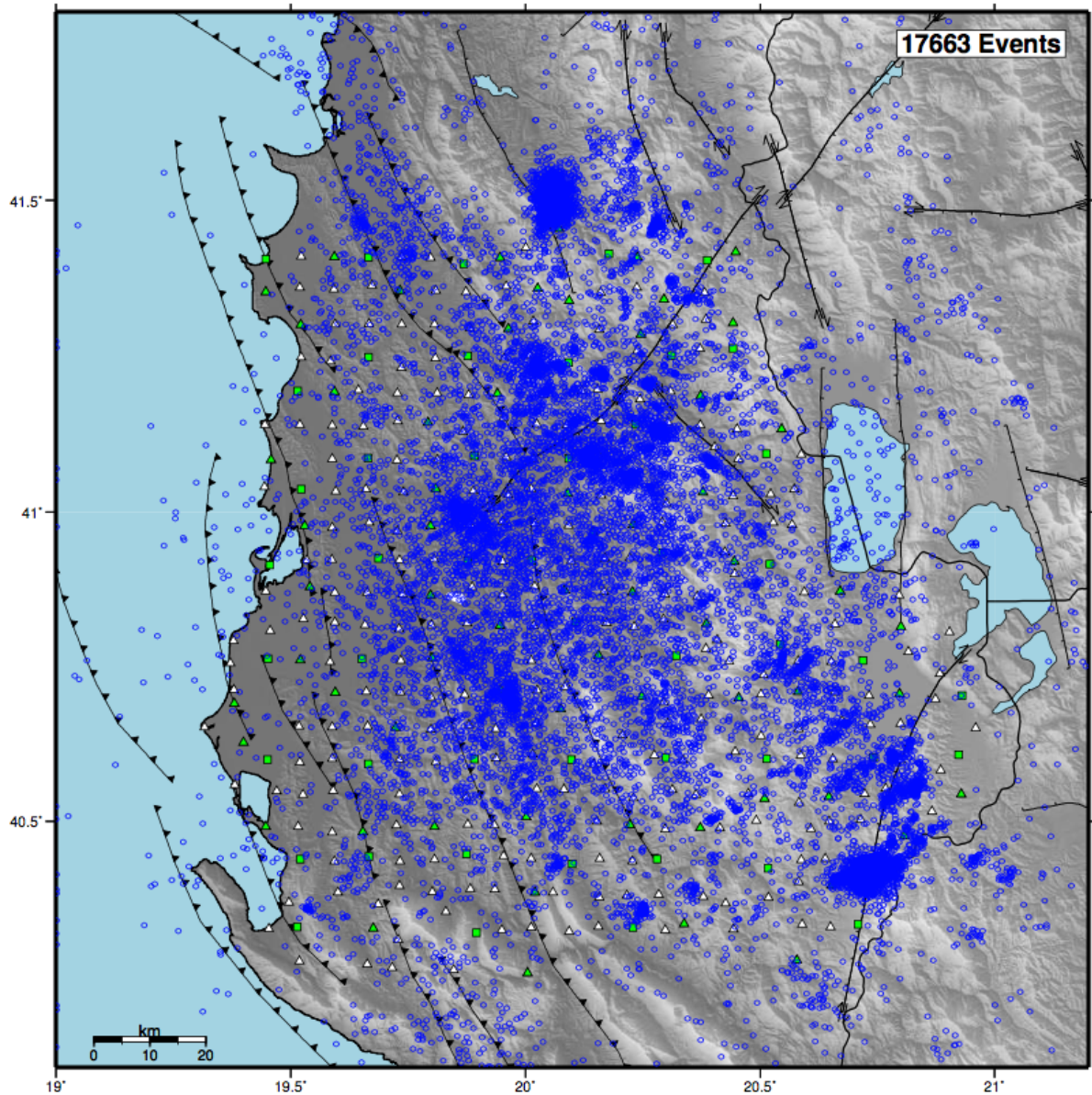
**Supplementary Figure 2.** PSD curves of vertical acceleration noise median for horizontal components of broadband (upper) and short-period (lower).



**Supplementary Figure 3.** PSD curves of vertical acceleration noise median for horizontal components of short-period stations installed during the second phase for receiver function lines.

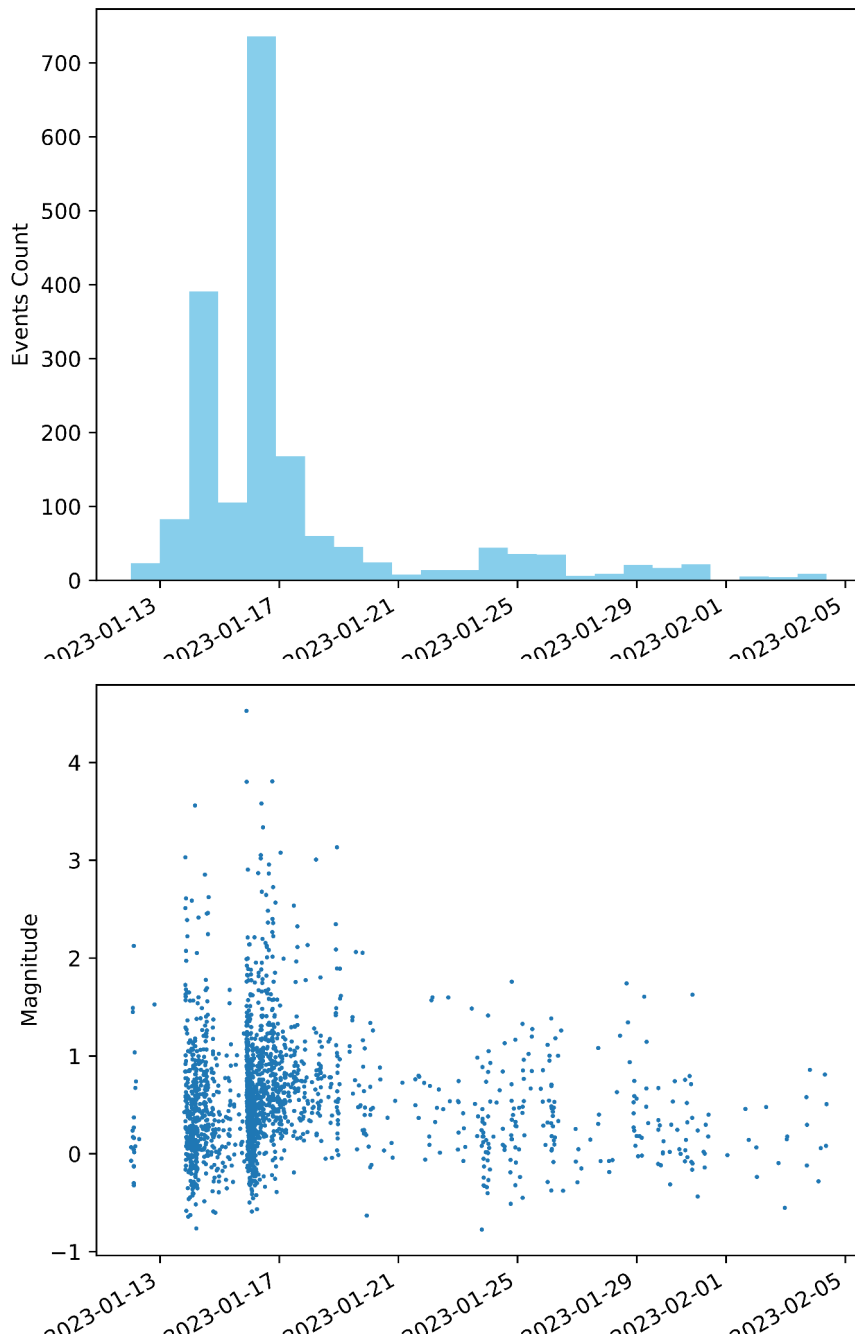


**Supplementary Figure 4.** Scatter plots of median noise amplitude versus elevation (left) and terrain slope (right) for each site. The slope was calculated as the maximum absolute value in the SW-NE direction. Relief model 1 arc-second from NASA JPL (2013).

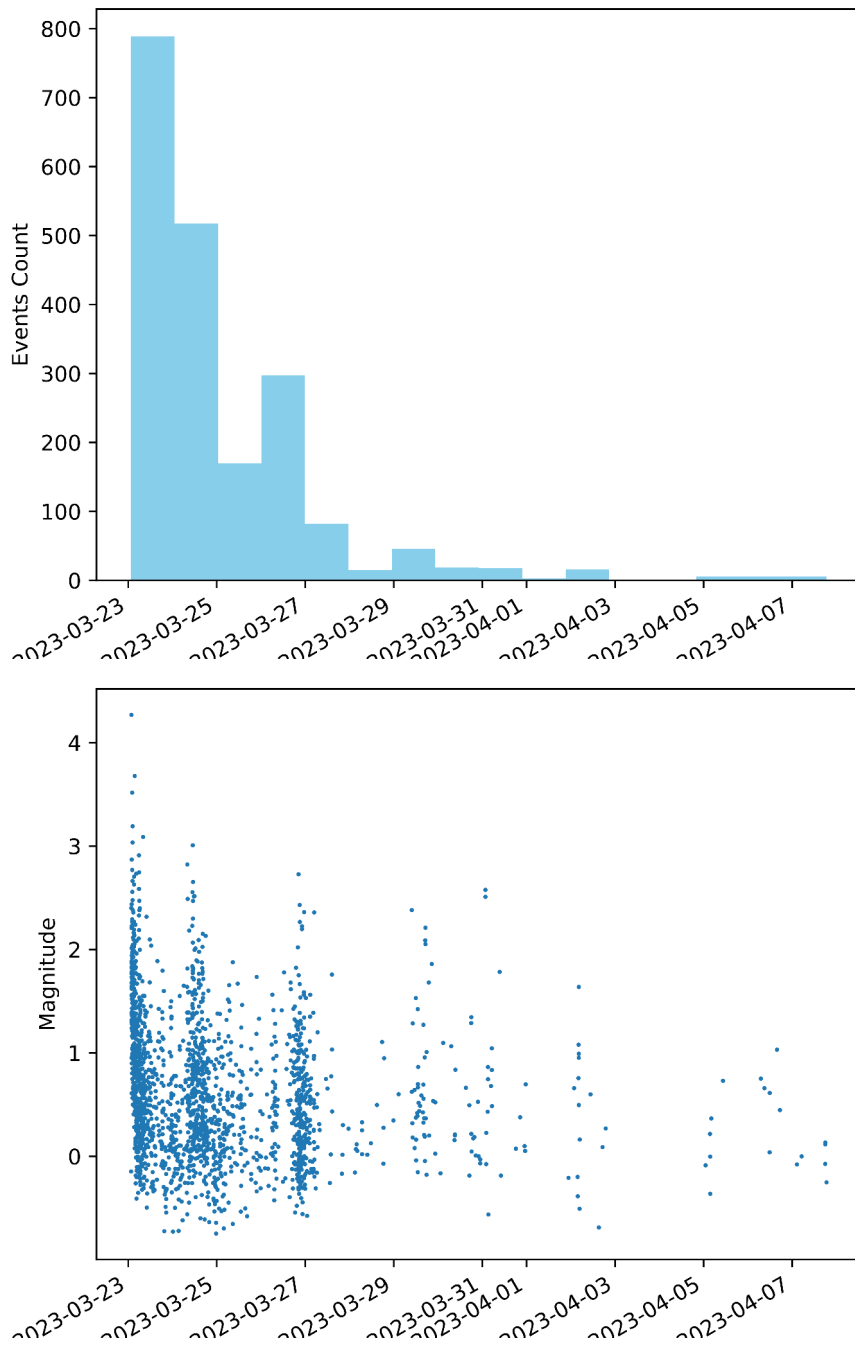


**Supplementary Figure 5.** Unfiltered complete catalogue with all ~18k events detected. For the present catalogue, only stations in green were used for seismicity detection.





**Supplementary Figure 6.** Temporal evolution of earthquakes (upper panel) and magnitudes (lower panel) for the Klos sequence during January 2023.



**Supplementary Figure 7.** Temporal evolution of earthquakes (upper panel) and magnitudes (lower panel) for the Erseke sequence during March 2023.